Supplementary Material

Cathode-Anode Spatial Division Photoelectrochemical Platform Based on One-Step DNA Walker for Monitoring of miRNA-21

Chuan Huang[#,a], Yunqing Liu[#,a], Yina Sun[a], Fengyi Wang[a], Shenguang Ge*[,a], Jinghua Yu[b]

[a]*Institute for Advanced Interdisciplinary Research, University of Jinan, Jinan 250022, P.R. China*

[b]*School of Chemistry and Chemical Engineering, University of Jinan, Jinan 250022, P.R. China*

Corresponding author:

Shenguang Ge (chm_gesg@163.com)

#These authors contributed equally to this work.

Table of contents

S1. Materials and apparatus

S1.1 Materials

The FTO slices were purchased from South China xiangcheng technology Co., Ltd (Shenzhen, China). Silver nitrate ($AgNO_3$), mercaptopropionic acid (MPA, 97%), N-(3-dimethylaminopropyl)-N'-ethylcarbodiimide (EDC) and N-hydroxysuccinimide (NHS) were obtained from Alfa Aesar China Ltd. Poly (diallyldimethylammonium chloride) (PDDA) (20%, w/w in water, molecular weight=200000-350000), indium (III) acetate, 6-mercaptohexanol (MCH), alkaline phosphate (ALP) and ascorbic acid 2-phosphate (AAP) were gained from Sigma-Aldrich Chemical Co. (USA). Monoethanolamine (MEA), thioglycolic acid (TGA), lead nitrate, $Na_2S·9H_2O$, hemin, ascorbic acid (AA) were purchased from Sinopharm Chemical Reagent Co., Ltd. (Shanghai, China). T7 Exo and 10 × NE buffer 4 were obtained from New England Biolabs Ltd. (Beverly, MA, USA). The 1 × TE buffer (10 mM Tris-HCl, 1.0 mM ethylenediaminetetraacetic acid (EDTA), pH 8.0) was employed for the dissolution of DNA oligonucleotides. DNA hybridization buffer (10 mM Tris-HCl, 1.0 mM EDTA, 1.0 M NaCl, pH 7.4), miRNA-21 DNA hybridization buffer (10 mM Tris-HCl,1.0 mM EDTA, 0.2 M NaCl, 10 mM $MgCl_2$, pH 7.4), the phosphate buffered solutions (PBS), pH 7.4 (0.1 M Na_2HPO_4, 0.1 M KH_2PO_4) and 0.1 M Tris−HCl (pH 7.4) buffer were used in this work. The biological chains (DNA and RNA fragments) used in the study were supplied by Sangon. (Shanghai, China). The sequences of the DNA and RNA used in this study were presented as follows:

Table S1. Oligonucleotides sequences used in this study.

name	sequences (from 5′ to 3′)
DNA1	TCAACATCAGTCTGATAA
DNA2	AACCGTTATCAGACTGATTTTTTTTTTTTTTTTTTTTTTTTTTTTTTTTTTT T-$(CH_2)_6$-NH_2
substrate-DNA	SH-$(CH_2)_6$-TCTGATAACGC-$(CH_2)_6$-NH_2
miRNA-21	UAGCUUAUCAGACUGAUGUUGA
miRNA-141	UAACACUGUCUGGUAAAGAUGG
let-7a	UGAGGUAGUAGGUUGUAUAGUU
miRNA-155	UUAAUGCUAAUCGUGAUAGGGGU

Note: Before using the substrate-DNA, the thiolated substrate-DNA was first pretreated with 10 mM tris(2-carboxyethyl)-phosphine for 1 h to cleave disulfide bond.

S1.2 Apparatus

The morphologies and structures were respectively characterized by scanning electron microscope (SEM) with Regulus-8100 (Hitachi hi-tech company, Japan). The transmission electron microscopy (TEM) images were obtained with a JEOL 4000 EX microscope (Japan). The high resolution transmission electron microscope (HRTEM) images were obtained with a Talos F200X transmission electron microscope (FEI, USA). The X-ray diffraction pattern (XRD) was investigated by an XRD- D8 FOCUS with Cu K_α source radiation at a scanning rate of 2° min^{-1} from 10° to 80°. The X-ray photoelectron spectroscopy (XPS) was performed using an ESCALAB 250XI electron spectrometer (Thermo Fisher Scientific, Waltham, MA, USA) with a focused monochromatic Al Kα X-ray source for excitation and a spherical section analyzer. The UV-visible (UV-vis) absorption spectra was tested on a UH-4150 ultraviolet-visible spectrophotometer (Hitachi, Japan). The fourier transform infrared (FTIR) spectrum was acquired on VERTEX 70 (Bruker, Germany). All electrochemical measurement was performed using a CHI 760D workstation (Chenhua, Shanghai, China);

S2. Characterization of $AgInS_2$ NPs

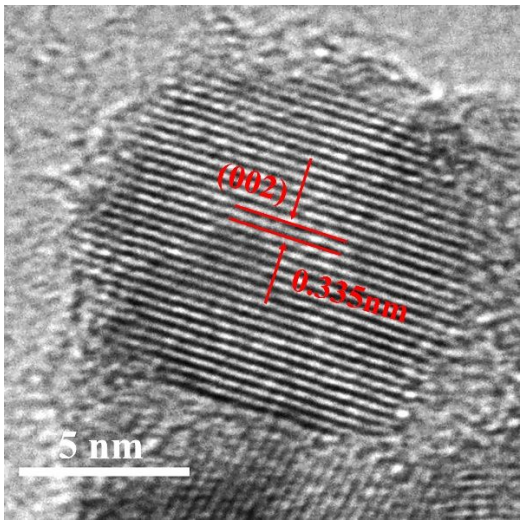

Figure S1. HRTEM image of $AgInS_2$ NPs.

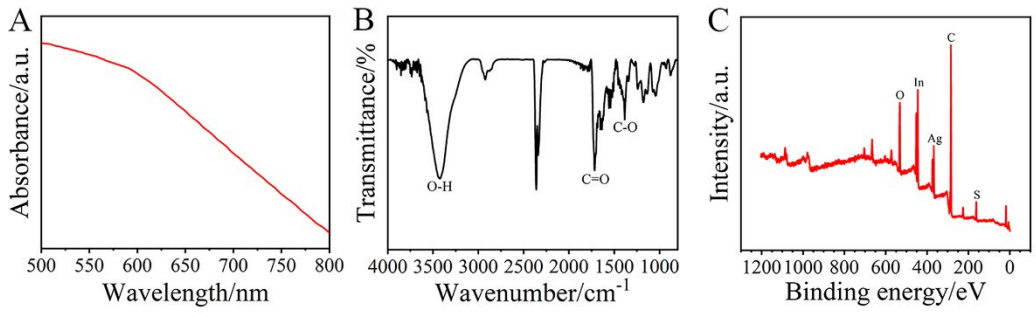

Figure S2. (A) UV–vis spectra of $AgInS_2$ NPs. (B) FT-IR spectrum of $AgInS_2$ NPs. (C) XPS survey scan of $AgInS_2$ NPs.

S3. Characterization of PbS QDs

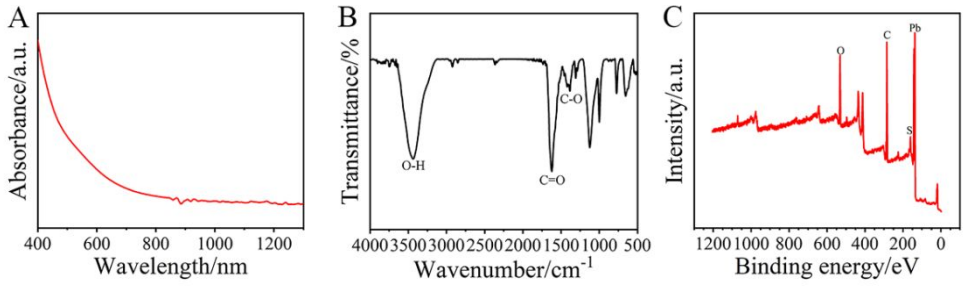

Figure S3. (A) UV–vis spectra of PbS QDs. (B) FT-IR spectrum of PbS QDs. (C) XPS survey scan of PbS QDs.

S4. Feasibility analysis of the one-step DNA walker amplification

The whole DNA Walker amplification response process was confirmed by native polyacrylamide gel electrophoresis (PAGE). As shown in Figure S4, miRNA-21, the substrate-DNA, the DNA2 and the DNA1 exhibited a distinct single band in lanes a, b, c and d, respectively. When DNA1 and DNA2 were annealed and hybridized to form the stable DNA arms, the lane e showed a bright band. Lane f exhibited two obvious bands of the DNA2, and the hybridization of DNA1/miRNA-21, suggesting that the miRNA-21 could hybridize with DNA1 to leave the DNA2 alone. In the presence of T7 Exo, lane g showed the bright band of DNA1 / miRNA-21 disappeared and a band parallel to lane a appeared, which proved that T7 Exo could digest DNA1 and release miRNA-21. Subsequently, two bright bands of lane h were observed which represented the hybridization bands of DNA2 / substrate-DNA and DNA1 / miRNA-21 respectively,

meaning that the single DNA2 left by the hybridization of miRNA-21 with DNA1 can hybridize with the substrate-DNA. As expect, after the addition of the T7 Exo into the above lane h mixture, lane i only showed parallel bands with Lane a and lane c, which proved that T7 Exo could also digest the substrate-DNA of the DNA2 / substrate-DNA hybrid strand to release DNA2. Therefore, we speculated that the one-step DNA walker amplification was occurred as expected.

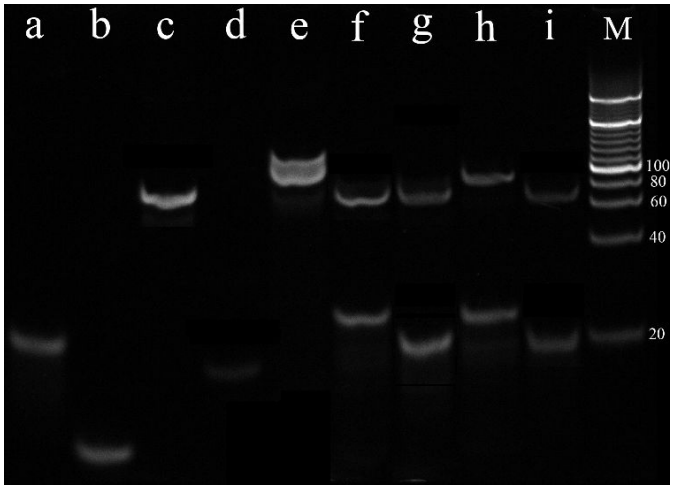

Figure S4. Native-PAGE analysis of different samples. (Lane a, 2 μM miRNA-21; Lane b, 2 μM substrate-DNA; Lane c, 2 μM DNA2; lane d, 2 μM DNA1; lane e, the annealed product of 2 μM DNA1 and 2 μM DNA2; lane f, 2 μM miRNA-21 and the annealed product of 2 μM DNA1 and 2 μM DNA2 (in the absence of T7 Exo); lane g, 2 μM miRNA-21 and the annealed product of 2 μM DNA1 and 2 μM DNA2 (in the presence of T7 Exo); lane h, 2 μM miRNA-21, 2 μM substrate-DNA and the annealed product of 2 μM DNA1 and 2 μM DNA2 (in the absence of T7 Exo); lane i, 2 μM miRNA-21, 2 μM substrate-DNA and the annealed product of 2 μM DNA1 and 2 μM DNA2 (in the presence of T7 Exo); lane M, DNA marker.

The TEM characterization was implemented to further clarify prove that the DNA attached onto Au NPs can be cleaved by T7 Exo. As shown in Figure S5, before the DNA Walker and T7 Exo digestion, Au NPs were well dispersed due to the electrostatic repulsion between the connected DNAs. However, after DNA Walker and T7 Exo digestion, the Au NPs aggregated significantly.[1,2] The comparison of the distribution of Au NPs directly proved that the 5' end of DNA attached onto Au NPs could be cleaved

by T7 Exo.

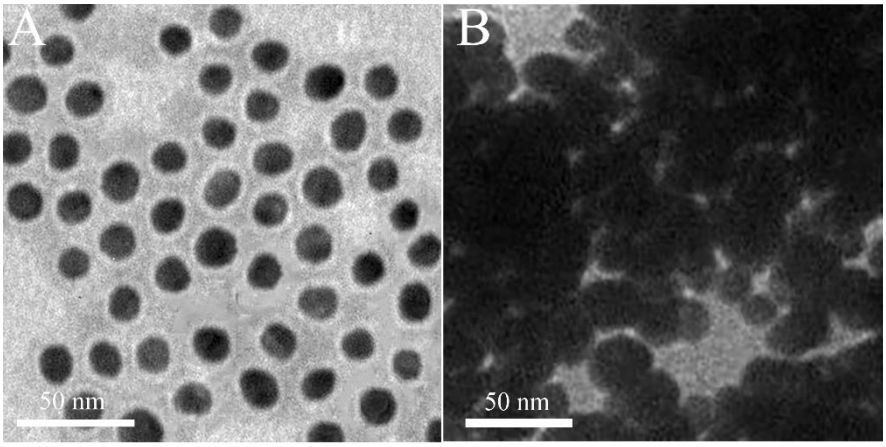

Figure S5. (A) TEM of the ALP-Au NPs-DNA before DNA walker and T7 Exo digestion. (B) TEM of the ALP-Au NPs-DNA after DNA walker and T7 Exo digestion.

S5. Condition optimization and characterization of the prepared photoelectrochemical biosensor

Since the prepared $AgInS_2$ NPs and PbS QDs were modified with carboxyl groups, the corresponding photoanode and photocathode can be connected to the amino group on the biological chain to form the platform equipped with One-Step DNA walker. In order to explore which photoelectrode was more suitable to be used in the designed One-Step DNA walker, based on the cathode-anode spatial division PEC platform, preliminary experiments were performed on the two photoelectrodes. As shown in the Figure 4A, after conducting a complete sensing experiment independently, the photocurrent of curve a larger than curve b, which proved that $AgInS_2$ photoanode has better stability and biocompatibility than PbS photocathode. The larger initial photocurrent could make the subsequent concentration gradient test results of miRNA-21 more accurate, so $AgInS_2$ photoanode was selected as the platform for carrying DNA walker, and PbS photocathode was used to amplify the photoelectrochemical signal. In order to obtain the optimal experimental property, the experimental conditions (pH, concentration of AAP, the incubation time of DNA swing arm, ALP-Au NPs-DNA and one-step DNA walker) were optimized (Figure S5). The AAP solution concentration played an important role in PEC biosensor. As seen from Figure S5E, the highest

photocurrent intensity was obtained at the solution concentration of 0.1 M, and higher or lower concentrations led to a decrease of photocurrent intensity. Therefore, 0.1 M AAP was selected for optimal concentration in the system.

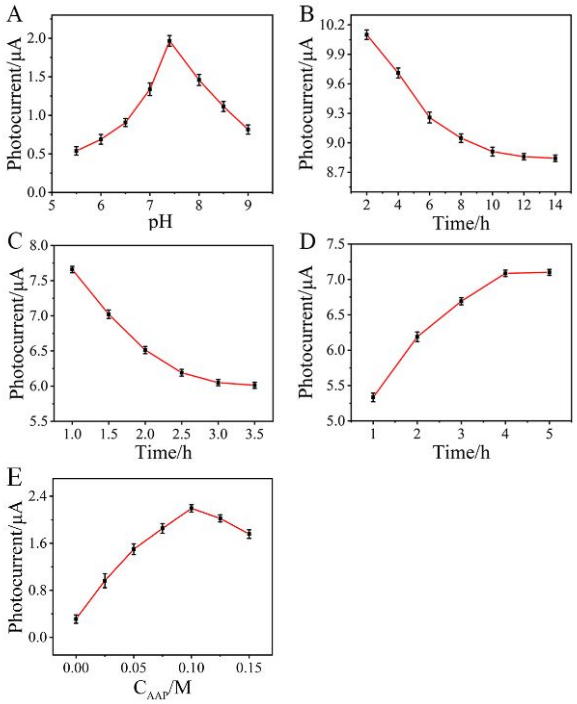

Figure S6. (A) pH of the 0.1 M PBS (10 nM miRNA-21). (B) incubation time of the DNA swing arm. (C) incubation time of the ALP-Au NPs-DNA. (D) incubation time of the one-step DNA walker. (E) concentration of AAP (1 nM miRNA-21).

Electrochemical impedance spectroscopy (EIS) characterization was carried out with a reversible electron probe $[Fe(CN)_6]^{3-/4-}$ to reflect the layer-by-layer fabrication of the PEC biosensor. Among them, the radius of the semicircle in the high-frequency region represented the charge transfer resistance (R_{et}), which could be used to preliminarily judge the load of the electrode. As shown in Figure 4B, the R_{et} value of the initial FTO/$AgInS_2$ electrode is comparatively small (curve a). Subsequently, when the FTO/$AgInS_2$ electrode was incubated with the DNA swing arm, the negatively charged DNA and $[Fe(CN)_6]^{3-/4-}$ repelled each other, making the R_{et} larger (curve b), that is, the difficulty of charge transfer between the electrode and electrolyte solution phase interface increased. Then, through the introduction of ALP-Au NPs-DNA with biomolecules and proteins, the R_{et} value enhanced significantly (curve c), which can be

mainly attributed to steric hindrance and insulation that gradually hindered the charge transfer process. Since then, the MEA was immobilized on the electrode resulted in an obviously augment of R_{et} value because of the nonconductive properties of MEA (curve d). Finally, with the simultaneous progress of DNA walker amplification and T7 Exo digestion, ALP-Au NPs-DNA was continuously cut from the electrode surface to decrease steric hindrance and acquire a reduction in R_{et} value (curve e). The PEC measurement also demonstrated the successful construction of the biosensor. As depicted in Figure 4C, the photocurrent response obtained by the photocathode and photoanode synergistically enhanced signal amplification strategy reached 11.1 μA (curve a). The amine-based DNA swing arm, ALP-Au NPs-DNA and MEA were then sequentially fixed on the $AgInS_2$ electrode surface through amidation reaction. As a result, the photocurrent responses decreased to 8.9 μA (curve b), 6.1 μA (curve c) and 4.7 μA (curve d) successively. The reduction of the photoelectrochemical effect was due to the continuous increase of the steric hindrance of the electrode surface through the step-by-step modification, which slowed down the transfer rate of photogenerated electrons and enhanced the carrier recombination rate. However, after incubating the reaction solution containing 100 nM miRNA-21 on the modified electrode, the DNA Walker used T7 Exo to remove the ALP-Au NPs-DNA with large steric hindrance on the electrode surface, so the photocurrent response was partially restored. The results of PEC and EIS were mutually corroborated, indicating that the PEC sensor for detecting miRNA-21 was successfully fabricated.

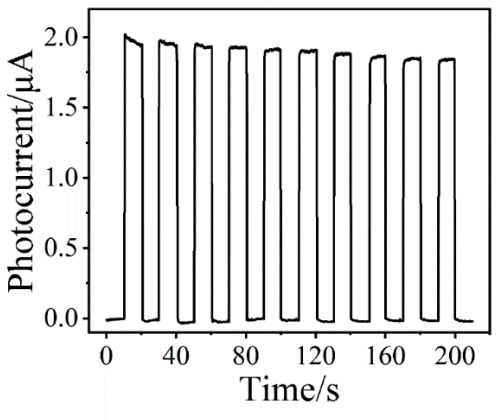

Figure S7. Reproducibility of the PEC biosensor (10 nM miRNA-21).

S6. Comparison of different methods for miRNA-21 detection

Table S2. Analytical performances of various methods towards miRNA-21

analytical method	LOD	linear range	Refs.
electrochemical	2.0 fM	10 fM to 1.0 nM	3
electrochemiluminescence	0.5 fM	1.0 fM to 1.0 nM	4
Raman	0.34 fM	1.0 fM to 10 nM	5
photoelectrochemical	0.31 pM	1.0 pM to 100 nM	6
chemiresistive	14.6 pM	10 pM to 100 nM	7
fluorescence	1.0 pM	1.0 pM to 1.0 nM	8
photoelectrochemical	3.4 fM	10 fM to 100 nM	This work

S7. Recovery tests for miRNA-21 in spiked human serum samples.

Table S3. Recovery tests for miRNA-21 in spiked human serum samples.

Samples	Added (pM)	Found (pM)	RSD (%) (n=5)	Recovery (%)
1	0.1	0.0951	3.7	95.1
2	1	1.023	2.5	102.3
3	10	9.872	4.1	98.7
4	100	103.4	2.9	103.4
5	1000	979.4	3.8	97.9

References

(1) Gao, Y.; Xu, S.; He, T.; Li, J.; Liu, L.; Zhang, Y.; Ge, S.; Yan, M.; Liu, H.; Yu J.

Ultrasensitive and Specific MicroRNA Detection via Dynamic Light Scattering of DNA Network Based on Rolling Circle Amplification. Sens. Actuators B Chem. 2020, 324, 128693−128702.

(2) Zhou, L.; Shen, R.; Ling, L.; Li, G. Sensitive DNA Detection by Polymerase Chain Reaction with Gold Nanoparticles. Anal. Chim. Acta 2018, 1038, 105−111.

(3) Fang, C. S.; Kim, K.-s.; Yu, B.; Jon, S.; Kim, M.-S.; Yang, H. Ultrasensitive Electrochemical Detection of miRNA-21 Using a Zinc Finger Protein Specific to DNA−RNA Hybrids. *Anal. Chem.* **2017**, *89*, 2024-2031.

(4) Feng, Q. M.; Shen, Y. Z.; Li, M. X.; Zhang, Z. L.; Zhao, W.; Xu, J. J.; Chen, H. Y. Dual-Wavelength Electrochemiluminescence Ratiometry Based on Resonance Energy Transfer between Au Nanoparticles Functionalized g-C_3N_4 Nanosheet and $Ru(bpy)_3^{2+}$ for microRNA Detection. *Anal. Chem.* **2016**, *88*, 937-944.

(5) Wen, S.; Su, Y.; Dai, C.; Jia, J.; Fan, G. C.; Jiang, L. P.; Song, R. B.; Zhu, J. J. Plasmon Coupling-Enhanced Raman Sensing Platform Integrated with Exonuclease-Assisted Target Recycling Amplification for Ultrasensitive and Selective Detection of microRNA-21. *Anal. Chem.* **2019**, *91*, 12298-12306.

(6) Chu, Y.; Wu, R.; Fan, G.-C.; Deng, A. P.; Zhu, J. J. Enzyme-Free Photoelectrochemical Biosensor Based on the CoSensitization Effect Coupled with Dual Cascade Toehold-Mediated Strand Displacement Amplification for the Sensitive Detection of MicroRNA-21. *ACS Sustain. Chem. Eng.* **2018**, *6*, 11633-11641.

(7) Huang, C. H.; Huang, T. T.; Chiang, C. H.; Huang, W. T.; Lin, Y. T. A Chemiresistive Biosensor Based on a Layered Graphene Oxide/Graphene Composite for the Sensitive and Selective Detection of Circulating miRNA-21. *Biosens. Bioelectron.* **2020**, *164*, 112320-112327.

(8) Huang, R.; Liao, Y.; Zhou, X.; Fu, Y.; Xing, D. Multiplexed Detection of MicroRNA Biomarkers from Tumor Cells and Tissues with a Homogeneous Nano-Photon Switch. *Sens. Actuators B Chem.* **2017**, *247*, 505-513.